Elastic and inelastic scattering of alpha particles from ^{40,44}Ca over a broad range of energies and angles*

Th. Delbar and Gh. Grégoire
Institut de Physique Corpusculaire, University of Louvain, Louvain-la-Neuve, Belgium

G. Paic
University of Louvain, Belgium
and Institut Ruder Boskovic, Zagreb, Yugoslavia

R. Ceuleneer, F. Michel, and R. Vanderpoorten†
Université de l'Etat, Mons, Belgium

A. Budzanowski, H. Dabrowski, L. Freindl, K. Grotowski, S. Micek, R. Planeta, and A. Strzalkowski
Jagellonian University and Institute of Nuclear Physics, Cracow, Poland

K. A. Eberhard
Sektion Physik, Universität München, D-8046 Garching West Germany
(Received 27 January 1978)

Angular distributions for α particle elastic scattering by ^{40,44}Ca and excitation of the 3.73 MeV 3^- collective state of ^{40}Ca were measured for incident energies ranging from 40 to 62 MeV. An extensive optical model analysis of these elastic scattering cross sections and other available data, using squared Woods-Saxon form factors, results in potentials with fixed geometry for both real and imaginary parts and depths with smooth energy behavior over a broad incident energy range. These results are discussed in the frame of the semi-classical approximation developed by Brink and Takigawa. The sensitiveness of the calculated elastic scattering cross sections to the real part of the potentials as a function of the projectile-target distance has been investigated by means of a notch test. Distorted-wave Born-approximation calculations for the excitation of the 3.73 MeV 3^- state of ^{40}Ca are presented.

[NUCLEAR REACTIONS ^{40}Ca$(\alpha,\alpha)(\alpha,\alpha')$, E_α= 40, 42, 44, 46, 48, 50, 54, 58, 62 MeV; ^{44}Ca(α,α) E_α= 40, 42, 46, 48, 50, 54, 58 MeV; measured $\sigma(\theta)$, $110° \leq \theta \leq 176°$; deduced optical model parameters and β_3 for the 3.73 MeV 3^- state of ^{40}Ca; enriched targets ^{40}Ca, ^{44}Ca.]

I. INTRODUCTION

Scattering of α particles from ^{40}Ca and from some other nuclei exhibits special features which are frequently called the anomalous large angle scattering (ALAS). As one can see from Figs. 1 and 2 the ^{40}Ca$(\alpha,\alpha)^{40}$Ca cross section is enhanced for angles larger than about 90°, while that for the ^{44}Ca$(\alpha,\alpha)^{44}$Ca behaves "normally." The enhancement of the back angle cross section depends regularly on the energy of α particles and the whole effect disappears above 55 MeV.

Many explanations of ALAS have been proposed: potential scattering, exchange effects, angular momentum mismatch, and quasimolecular resonances. A more detailed description of ALAS, discussion of its possible explanations, and a comprehensive list of references can be found in one of several review articles.[1,2,3]

Some analyses of ALAS performed for targets with A around 40 have given rise to controversy. For instance, some authors suggest a purely potential description,[4-7] whereas other groups disagree with this statement.[8-11] In an attempt to clarify this situation backward angular distributions for the ^{40,44}Ca$(\alpha,\alpha)^{40,44}$Ca elastic scattering and for the excitation of the 3.73 MeV 3^- collective state in ^{40}Ca have been measured for incident energies ranging from 40 up to 62 MeV (Sec. II). The elastic scattering data, together with data obtained by Gaul *et al.*,[12] Löhner *et al.*,[11] Eickoff *et al.*,[13] Goldberg,[14] and Brissaud and Brussel[15] were analyzed using the optical model with squared Woods-Saxon form factors. Angular distributions for excitation of the 3^- state of ^{40}Ca were calculated using the distorted-wave Born approximation (DWBA). Results of our analysis are presented in Sec. III and are discussed in Sec. IV.

II. EXPERIMENTAL METHOD

The experiment was performed at the Louvain-la-Neuve isochronous cyclotron. The incident α-particle beam was focused on self-supporting targets located in the center of a 1 m diameter scattering chamber. Data were taken at eight incident energies 40, 42, 44, 46, 48, 50, 54, and 58 MeV, for both ^{40}Ca and ^{44}Ca in the backward hemisphere for center-of-mass scattering angles between 110° and 176°. For ^{40}Ca, measurements were also made at 62 MeV in the same angular range. The accuracy of the beam energy given by the cyclotron was checked many times by the crossover method and is consistently of the order of ±100 keV. The energy spread of the beam is of the order of 0.3%. The size of the beam spot on the target is 3×3 mm.

The isotopically pure ^{40}Ca and ^{44}Ca targets were supplied by the Munich group. Their thicknesses were measured both by weighing and by transmission of α particles emitted by an ^{241}Am source. Measurements by the two methods were found to agree within 10%. The target thicknesses were, respectively, 0.78 and 2.04 mg/cm^2 for the ^{40}Ca and ^{44}Ca isotopes. All targets contained some carbon (0.21 mg/cm^2) and oxygen (0.26 mg/cm^2). The thicknesses of these contaminants were estimated by comparison with the data published by Van Oers *et al.*[16] and by Baron *et al.*[17] Within the accuracy of our measurements, the amount of carbon and oxygen did not vary during the experiment. This allowed us to obtain backward angular distributions for ^{12}C$(\alpha,\alpha)^{12}$C and ^{16}O$(\alpha,\alpha)^{16}$O elastic scattering in the same energy range as for the calcium experiment.

The detection system consisted of seven Si(Li) semiconductor detectors cooled to about −20°C. They were manufactured at the Department of Physical Electronics, IFUJ, Cracow, and their depletion depths were about 3000 μm. These detectors are placed 10° apart on a turntable rotatable around the target axis. The accuracy of the detection angles was checked by Rutherford scattering on both sides of the beam axis and was found to be accurate to ±0.2°. The solid angles were measured by Rutherford scattering of 15 MeV α particles from a thin gold target and were found to agree with the geometrical estimate. All solid angles were of the order of 0.3 msr.

Each detector amplifier chain was connected to one input of a multiplexer, the output of which was fed into a 1024 channel ADC. Energy calibrations were done on-line by placing ^{212}Bi α-particle sources in front of each detector. The overall full width at half maximum for the elastic peak was about 150 keV. The deadtime in each chain was monitored continuously with a random pulser. The beam intensity was adjusted to get deadtime corrections less than 10%. Data are on deposit in PAPS.

The errors on the data points shown in Figs. 1–3 are statistical only. The absolute cross sections are estimated to be accurate within ±15%.

III. OPTICAL MODEL ANALYSIS

An optical model with Woods-Saxon squared form factors for both real and imaginary parts of the potential was used to describe the elastic scattering data. The use of the Woods-Saxon squared form factor or similar forms is becoming increasingly popular as they have been shown to be superior to the traditional Woods-Saxon parametrization at low[19] as well as at high incident energies.[14] A Woods-Saxon squared form factor has recently been used by Chang *et al.*[20] in their extensive analysis of the ^{40}Ca$(\alpha,\alpha)^{40}$Ca and ^{58}Ni$(\alpha,\alpha)^{58}$Ni scattering at small and intermediate angles. It was also recently applied by Budzanowski *et al.*[21] for both real and imaginary parts of the potential, yielding excellent fits to the ^{58,60}Ni$(\alpha,\alpha)^{58,60}$Ni data in the broad energy range from 26.5 up to 139 MeV and for scattering angles approaching 180°. In addition, it has been demonstrated that the energy break in the parameters found by Put and Paans[22,23] in their extensive optical model analysis of ^{90}Zr(α,α) data could be eliminated by the choice of a convenient real form factor of the folding[24,25] or of the squared Woods-Saxon type.[26] A Woods-Saxon form factor raised to a variable power ν was used by Michel and Vanderpoorten[7] in the study of ^{40}Ca$(\alpha,\alpha)^{40}$Ca data covering the whole angular range. The optimal value $\nu=2.65$ was found in this analysis. This allowed a very convenient description of the complicated energy dependence of the backward enhancement from 18 up to 50 MeV incident energy.

Finally double folding type calculations suggest that the shape of the real part of the α-nucleus optical potential is different from the Woods-Saxon form[27] and a theoretical study[25] of the influence of antisymmetrization effects in α-particle scattering indicates that the sum of the direct and local exchange equivalent parts of the α-nucleus interaction can be adequately represented by a squared Woods-Saxon form factor.

Two parametrizations A and B of the optical potential were used in the optical model analysis of the experimental data for ^{40}Ca. In the A parametrization, six-parameter automatic searches using the standard χ^2 technique were first carried out with the new data taken at Louvain-la-Neuve for the ^{40}Ca nuclei; the optical potential was defined by the expression

$$V(r)=V_C(r)-U_0f^2(r,d_1,b_1)-iW_0f^2(r,d_2,b_2)\,, \tag{1}$$

where

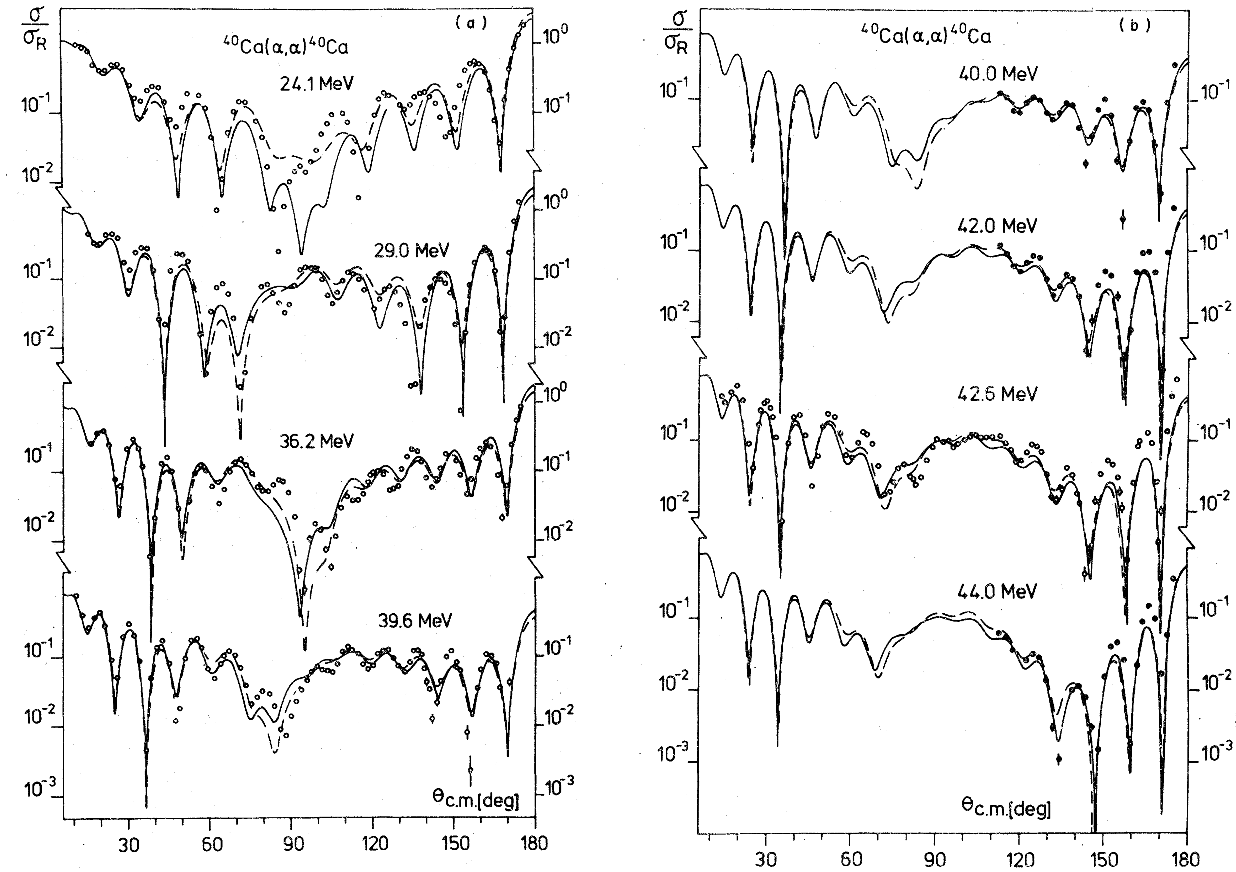

FIG. 1. Comparison of experimental data for ${}^{40}Ca(\alpha, \alpha){}^{40}Ca$ with theoretical cross sections calculated with the potential A (dotted curve) and potential B (full line). Only error bars exceeding the size of the data points are marked. (a) Open circles, data from Refs. 11 and 12. (b) Open circles, data from Ref. 11. (c) Filled circles, data from this work, open circles, data from Ref. 11. (d) Filled circles, data from this work, open circles, data from Ref. 11. (e) Open circles, data from Refs. 13–15.

$$f(r, d_i, b_i) = \left(1 + \exp\frac{r - d_i A_T^{1/3}}{b_i}\right)^{-1}, \qquad (2)$$

and $V_C(r)$ is the Coulomb potential due to an uniformly charged sphere of the radius $1.3A_T^{1/3}$ fm. For the Woods-Saxon-squared form factor the halfway radius $R_{1/2}$ and the 10–90% distance t_{10-90} describing the diffuseness of the potential in its surface part are connected with the parameters d and b as follows[21]:

$$R_{1/2} = r_{1/2}A_T^{1/3} = dA_T^{1/3} + b\ln(\sqrt{2} - 1),$$
$$t_{10-90} = b\ln\left(\frac{\sqrt{10} - 1}{\sqrt{10/9} - 1}\right). \qquad (3)$$

The searches were restricted to the potential family with a real volume integral per nucleon pair $J_U/4A_T$ of the order of 370 MeV fm^3; this is the only one fitting the data at high energy, as was shown by Goldberg in his optical model analysis of the ${}^{40}Ca$ data at 141.7 MeV incident energy.[14]

Very good agreement was obtained at each energy on the experimentally investigated angular range; the resulting parameters are listed in Table I. Examination of Table I shows that the parameters of the real part of the potential display a remarkable stability at all energies. Although the individual parameters of the imaginary part are more scattered, its volume integral is seen to increase quite smoothly with incident energy.

After allowing for a monotonic decrease of the real volume integral of the potential with energy, calculations performed with parameters extrapolated from Table I turned out to give a good overall description of experimental distributions taken on the whole angular range both at lower and at higher energies. It was therefore decided to fix the geometrical parameters of the real part of the potential and to impose a linear decrease of its depth with energy, and the slope is determined by examination of the high-energy data.

In view of the well-known ambiguities in the

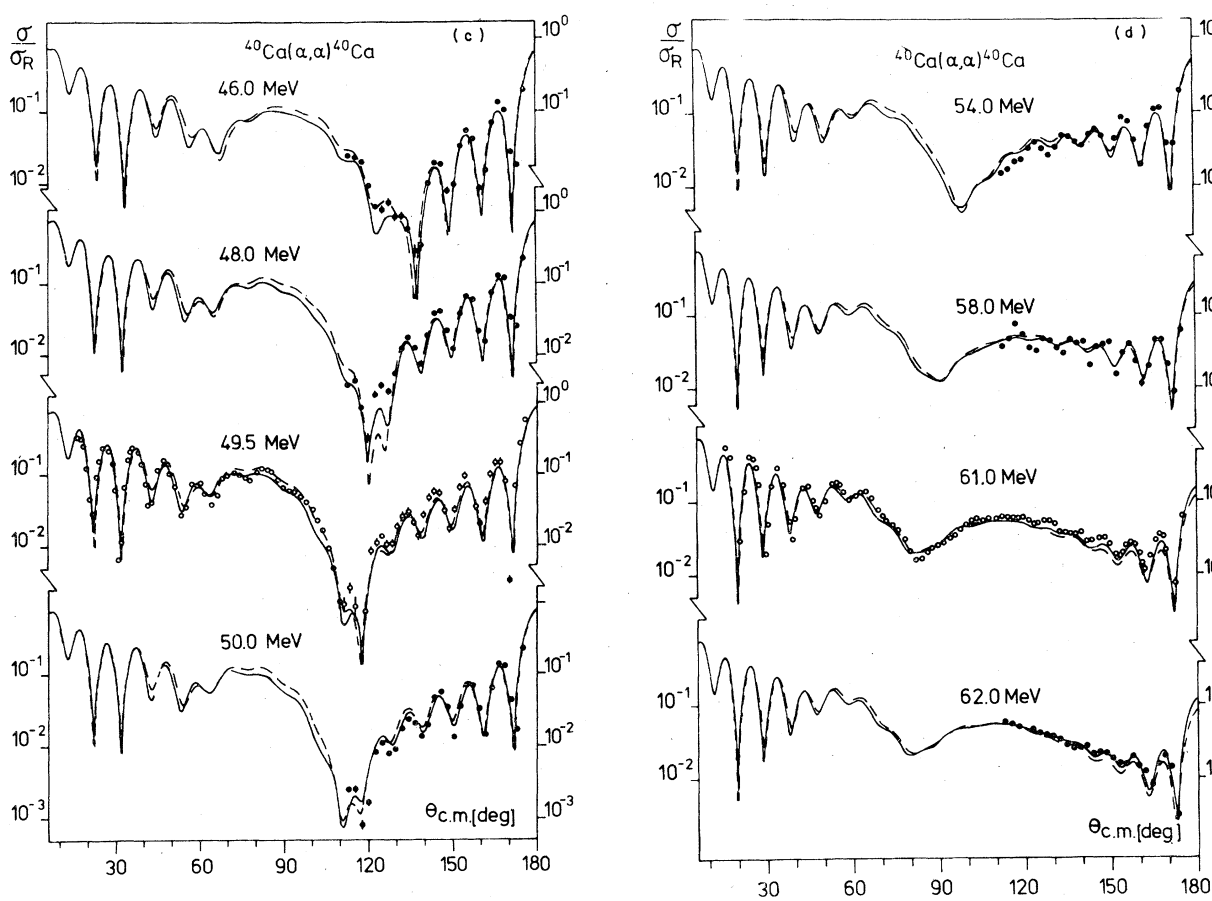

FIG. 1. (*Continued*)

imaginary part of the optical model potential at low energy[28] the radius and the diffuseness of the potential were fixed at values obtained by fitting the higher energy data.

The parameters of the potential constructed in this way are

$$U_0 = 198.6\,(1-0.00168\,E_\alpha)\ \text{MeV}\,,\quad d_1 = 1.37\ \text{fm}\,,\quad b_1 = 1.29\ \text{fm}\,,\quad d_2 = 1.75\ \text{fm}\,,\quad b_2 = 1.00\ \text{fm}\,. \tag{4}$$

Fitting the only remaining free parameter W_0 to experiment indicated that its energy variation can adequately be represented by the following linear prescription for $E_\alpha < 62$ MeV:

$$W_0 = (2.99 + 0.288\,E)\ \text{MeV}\,. \tag{5}$$

It is difficult to trace the energy behavior of W_0 above 62 MeV, as only three angular distributions widely separated in energy (viz., $E_\alpha = 100$, 141.7, and 166 MeV), are experimentally available; at these energies, W_0 took on the values 25.14, 23.25, and 22.88 MeV.

Equations (1)–(5) together with the above prescription for W_0 for $E_\alpha > 62$ MeV define the potential A. Angular distributions calculated with the potential A are compared with all experimental data in Fig. 1.

The parametrization B was used in a global search performed simultaneously for all energies of incident α particles in the way applied recently for the ^{58,60}Ni$(\alpha,\alpha)^{58,60}$Ni) case.[21] The potential B had the form

$$V(r) = V_C(r) = Uf^2(r, d_1, b_1) - i\Big[W_v f^2(r, d_2, b_2) - 4b_3 W_D \frac{d}{dr} f^2(r, d_3, b_3)\Big]\,, \tag{6}$$

where $f(r, d_i b_i)$ is given by expression (2).

Parameters of the potential B were assumed to depend on incident α particle energy in the following way:

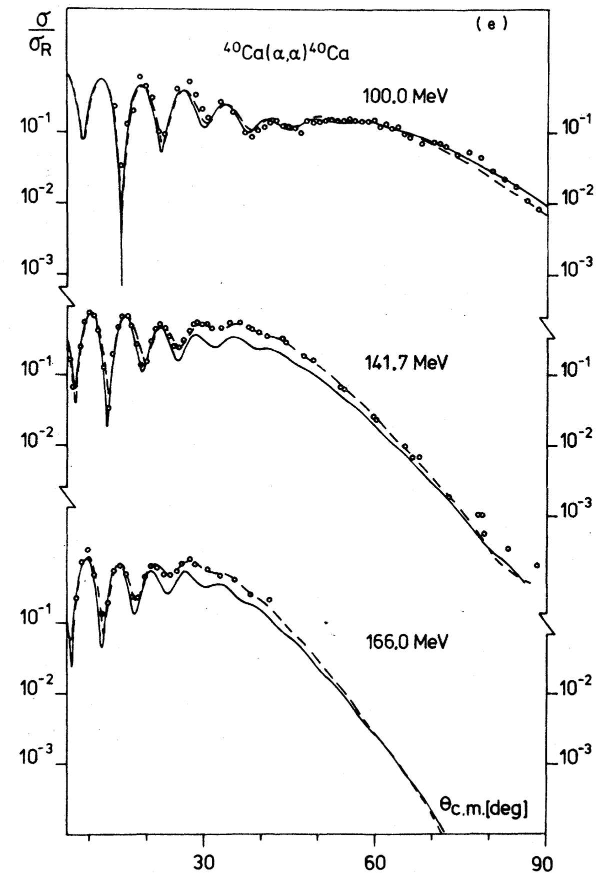

FIG. 1. (*Continued*)

$$U = A_1 + A_2 E_\alpha ,$$
$$W_v = A_3 - A_4 \exp(-A_5 E_\alpha) , \qquad (7)$$
$$W_D = A_6 \exp(-A_7 E_\alpha) + A_8 .$$

All the geometrical parameters were assumed to be energy independent. As for the potential A, the discrete ambiguities were avoided by fixing the depth of the real potential from fits at high incident energies.[14] Extrapolation towards lower incident energies was made keeping in mind a reasonable slope of the energy dependence of the real potential. Parameters of the potential B are given in Table II; results of the global search are presented in Fig. 1. A similar global search using the parametrization B was performed for ^{44}Ca. Resulting parameters are given in Table II and corresponding cross sections are displayed in Fig. 2.

IV. DISCUSSION

As one can see from Figs. 1 and 2 it is possible to get a reasonable description of the energy behavior of the elastic scattering of α particles from both ^{40}Ca and ^{44}Ca nuclei using the optical model with Woods-Saxon-squared form factors of the potential. In particular, the energy dependence of the anomalous large angle scattering from ^{40}Ca is properly reproduced. In addition, DWBA calculations for excitation of the 3.73 MeV 3^- state in ^{40}Ca performed with the same potentials and with the value of the collective deformation parameter fixed at $\beta_3 = 0.22$ give a good description of the rapid energy variation of experimental data (Fig. 3). This value of β_3 is compatible with previous estimates (see references quoted in Ref. 7).

Figure 4 presents the energy dependence of the volume integrals calculated for the real (J_U) and imaginary (J_W) parts of the potentials A and B, respectively. The volume integrals of real parts show the following linear dependence:

$$J_U/4A_T = (383.8 - 0.64E_\alpha)\ \mathrm{MeV\,fm^3}, \quad ^{40}\mathrm{Ca\text{-}potential}\ A ,$$
$$J_U/4A_T = (378.9 - 0.49E_\alpha)\ \mathrm{MeV\,fm^3}, \quad ^{40}\mathrm{Ca\text{-}potential}\ B ,$$
$$J_U/4A_T = (368.2 - 0.31E_\alpha)\ \mathrm{MeV\,fm^3}, \quad ^{44}\mathrm{Ca\text{-}potential}\ B .$$

The energy dependences found here are comparable to those found in other optical model studies

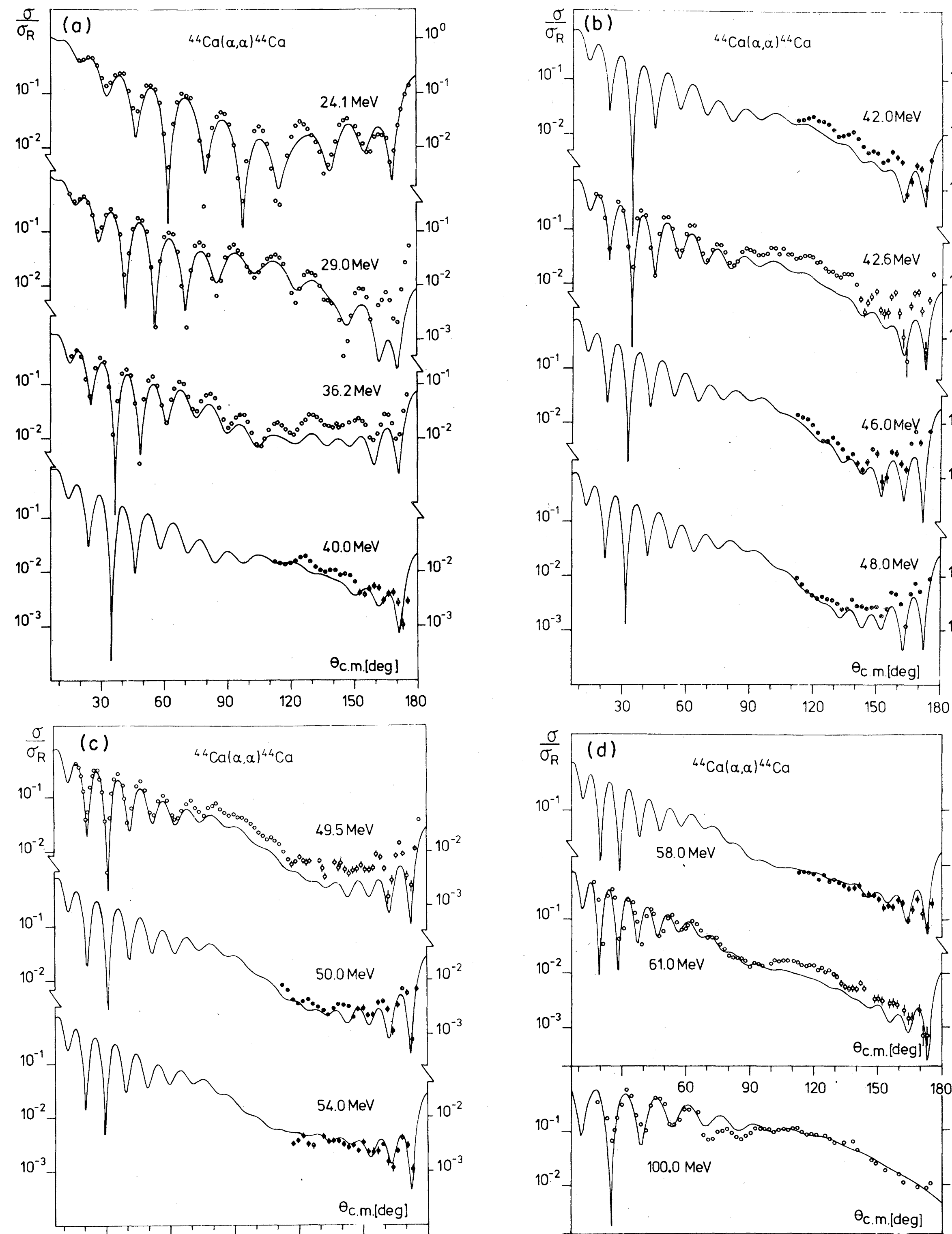

FIG. 2. Comparison of experimental data for ^{44}Ca(α, α)^{44}Ca with theoretical cross sections calculated with the potential B (full line). Only error bars exceeding the size of the data points are marked. (a) Filled circles-data from this work; open circles-data from Refs. 11 and 12. Only error bars exceeding the size of the data points are marked. (b) Filled circles data from this work, open circles data from Ref. 11. (c) Filled circles, data from this work, open circles, data from Ref. 11.. (d) Filled circles, data from this work, open circles data from Refs. 11 and 13.

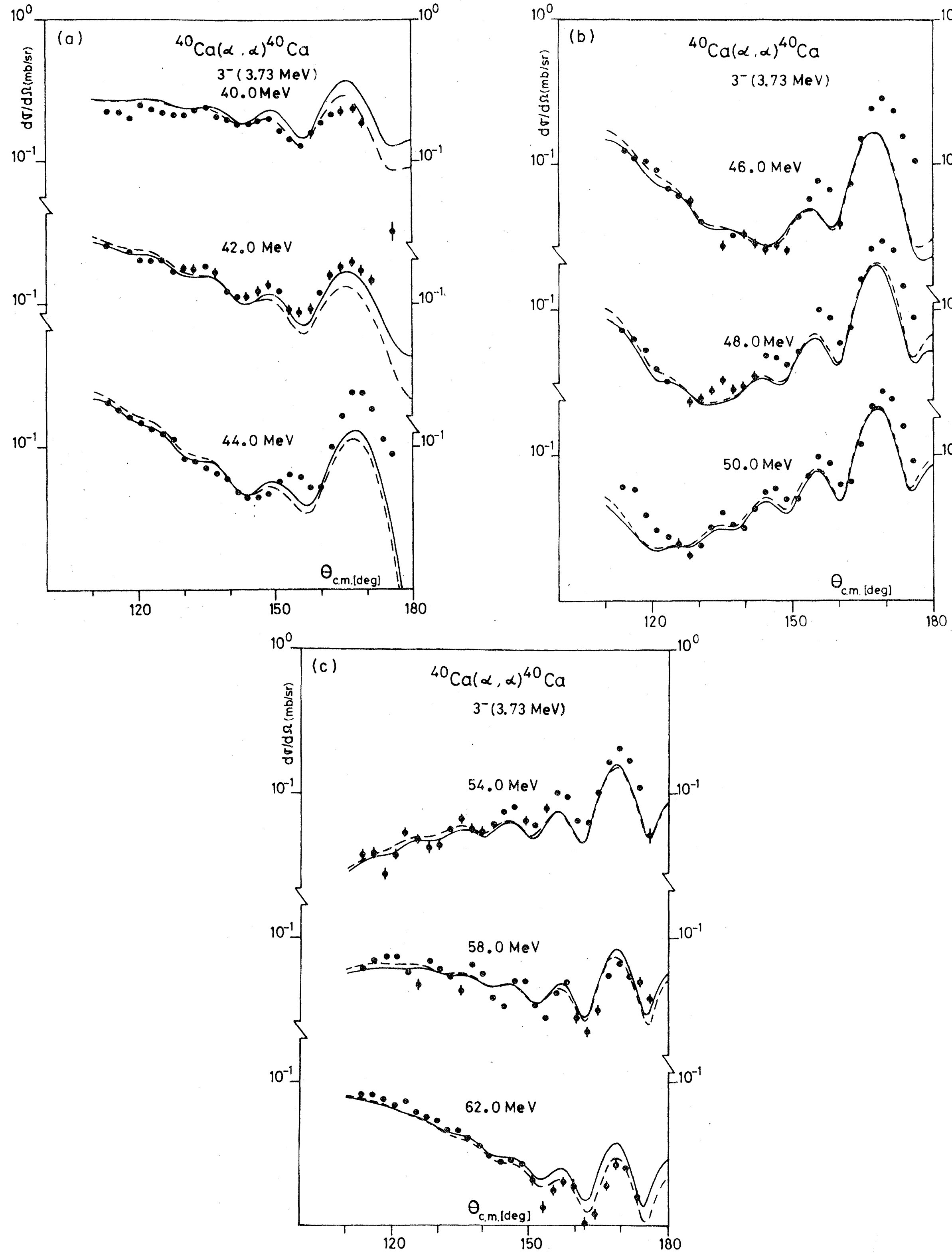

FIG. 3. (a)–(c) Comparison of experimental data obtained in this work for ^{40}Ca(α, α')^{40}Ca (filled circles) with the results of the DWBA calculations using potential A (dotted curve) and potential B (full line). Only error bars exceeding the size of the data points are marked.

TABLE I. Best fit parameters and volume integrals obtained in the framework of parametrization A, defined by Eqs. (1) and (2). Energies are in MeV, lengths in fm, volume integrals in MeV fm^3.

E_α	U_0	d_1	b_1	W_0	d_2	b_2	$\frac{J_U}{4A_T}$	$\frac{J_W}{4A_T}$
40	181.0	1.38	1.30	25.0	1.44	1.77	362.1	60.0
42	180.9	1.37	1.28	22.9	1.50	1.61	352.5	69.6
44	177.8	1.38	1.29	22.0	1.56	1.37	354.6	62.8
46	180.0	1.41	1.31	23.0	1.61	1.48	378.1	71.8
48	175.7	1.39	1.28	23.6	1.61	1.37	354.2	73.0
50	179.0	1.39	1.27	17.5	1.75	0.93	358.7	72.4
54	182.6	1.36	1.27	22.7	1.65	1.18	346.0	76.1
58	187.6	1.36	1.31	22.9	1.70	0.52	355.5	94.0
62	182.6	1.35	1.29	21.4	1.72	0.94	338.7	83.4

for both light and heavier targets and in microscopic model estimates.[20,21,24,25,26,29]

Whereas volume integrals of the real part of the potential are similar for both ^{40}Ca and ^{44}Ca nuclei the volume integrals for the imaginary potential differ considerably. As can be seen, the absorption in the $^{40}\mathrm{Ca}+\alpha$ scattering is strongly reduced for lower incident energies. For higher energies, α particles are always less absorbed in ^{40}Ca than in ^{44}Ca but the energy dependence of both absorptions looks similar. This reflects the known fact that although ALAS in ^{40}Ca does not exist above 55 MeV, cross sections for $^{44}\mathrm{Ca}(\alpha,\alpha)^{44}\mathrm{Ca}$ are always smaller than for $^{40}\mathrm{Ca}(\alpha,\alpha)^{40}\mathrm{Ca}$ in the whole region of scattering angles.[8]

Figure 5, where the function $r^2W(r)$ is presented suggests some additional information on the absorption of α particles in ^{40}Ca and ^{44}Ca in the framework of the potential B. This function is proportional, in the first order perturbation theory,[30] to the amount of flux of incident α particles absorbed from the entrance channel in a spherical layer at a distance r from the center of the nucleus. As one can see, at 30 MeV incident energy, most of the absorption in the ^{44}Ca nucleus is located by the derivative term of the imaginary potential W_D between about 3 and 6 fm while in ^{40}Ca the absorption is shifted slightly toward the center of the nucleus. Figure 5 displays also the effective charge distribution $\rho_N(r)$ of the $f_{7/2}$ neutrons[31] multiplied by r^2. It seems that the space distribution of the absorption in ^{44}Ca is to

TABLE II. Numerical values of the global search parameters defined for the potential B by Eqs. (6) and (7). The geometry parameters for potential B are defined by Eqs. (1), (2), and (3). Values of $r_{1/2}$ and t_{10-90} for the potential A and B are also presented. Energies are in MeV, lengths in fm.

	A_1	A_2	A_3	A_4	A_5	A_6	A_7	A_8
^{40}Ca	179.9	−0.233	26.3	49.5	0.0319	226.2	0.1051	2.27
^{44}Ca	171.8	−0.146	29.6	51.6	0.0414	79.95	0.0683	1.53

Geometry parameters

	d_1	b_1	d_2	b_2	d_3	b_3
^{40}Ca	1.41	1.24	1.79	1.00	0.620	1.04
^{44}Ca	1.42	1.25	1.75	0.934	1.36	0.378

Potential B

	$r_{1,1/2}$	$t_{1,10-90}$	$r_{2,1/2}$	$t_{2,10-90}$
^{40}Ca	1.09	4.57	1.53	3.69
^{44}Ca	1.11	4.61	1.52	3.44

Potential A

	$r_{1,1/2}$	$t_{1,10-90}$	$r_{2,1/2}$	$t_{2,10-90}$
^{40}Ca	1.04	4.76	1.49	3.69

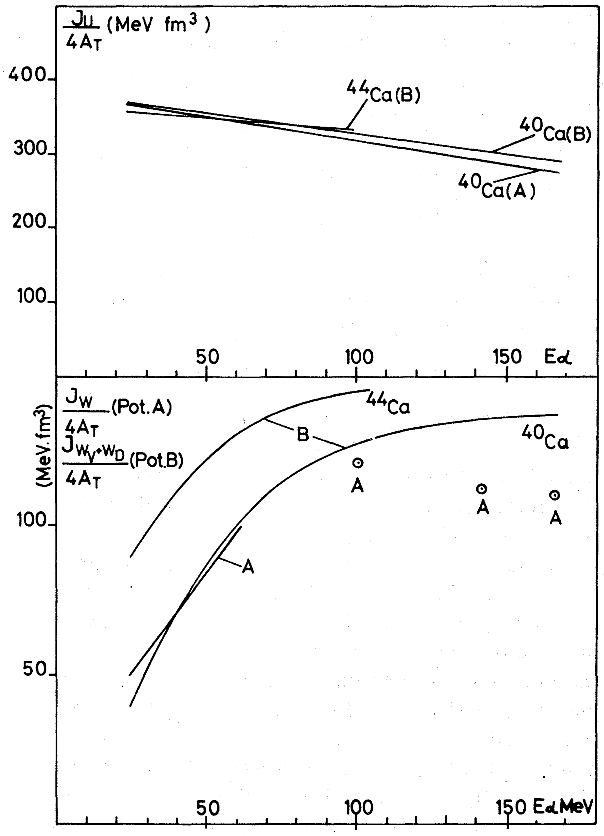

FIG. 4. Energy dependence of volume integrals of the real part (upper picture) and imaginary part (lower picture) of the potentials A and B, respectively.

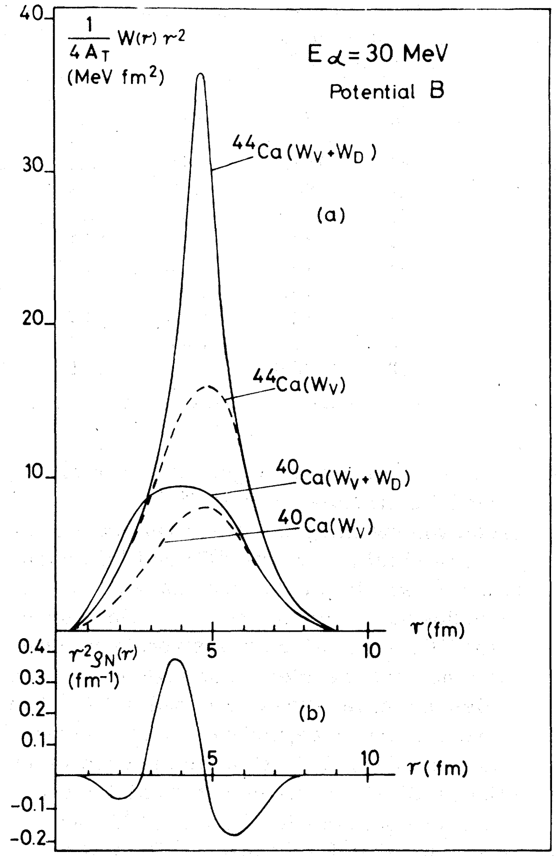

FIG. 5. Amount of flux of incident α particles absorbed from the entrance channel in a spherical layer at a distance r from the center of the nucleus (picture a). Picture b displays the effective charge distribution $\rho_N(r)$ of the $f_{7/2}$ neutrons in the same spherical layer (Ref. 31).

some extent correlated with the $f_{7/2}$ neutron shell.

Parametrization A is simpler than parametrization B. It is somewhat less successful in reproducing experimental data for lower scattering energies but it seems to work better above 100 MeV, where both potentials have a similar form with the exception of the energy dependence of W.

A useful tool for studying the properties of optical potentials is the three-turning point WKB approximation of Brink and Takigawa[32,33] for complex potential scattering. In this approximation, the semiclassical scattering amplitude $f^{sc}(\theta)$ splits into two parts $f_I(\theta)$ and $f_B(\theta)$. The barrier term f_B is essentially the usual WKB scattering amplitude with reflection on the external turning point, including a (generally small) correction for barrier penetration. The internal contribution f_I describes reflection on the internal classical turning point which is reached by tunnelling of the incoming particle through the barrier of the effective (nuclear + Coulomb + centrifugal) potential. It proved to be convenient to study the quantities $\sigma_I = |f_I|^2$ and $\sigma_B = |f_B|^2$, the comparison of which with the cross-section $\sigma^{sc} = |f^{sc}|^2$ gives insight into the relative magnitude and phase of f_I and f_B.

As an illustration, σ^{sc}, σ_I, and σ_B, computed for the potential A of the ^{40}Ca for $E_\alpha = 36.2$ and 49.5 MeV are plotted in Fig. 6. These energies were chosen because they allow comparison with experiment over a wide angular range, and because they display very different behaviors of the cross section. The same calculation performed with the potential B yields very similar results.

One sees that the barrier term f_B dominates at small scattering angles and becomes more important as energy increases. On the other hand, the internal contribution f_I dominates at large angles and low energy; in the cases of Fig. 6, it interferes constructively with f_B at forward and backward angles, with both components nearly canceling each other at intermediate angles (around $\theta = 95°$ at 36.2 MeV, $\theta = 120°$ at 49.5 MeV). One understands, in view of Fig. 6, why a careful choice of the potential form factor is important in order to obtain smoothly varying potential para-

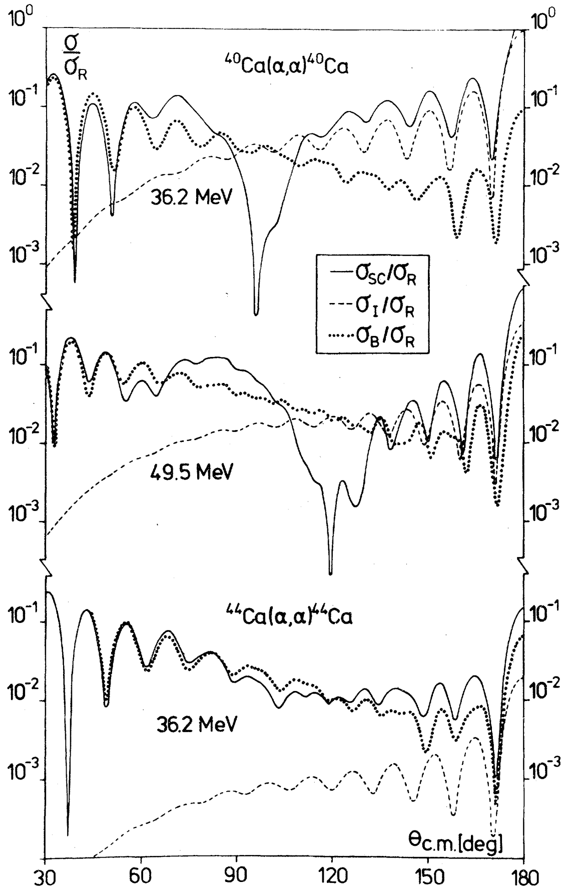

FIG. 6. Angular distribution σ_{sc} calculated from the semiclassical scattering amplitude together with angular distributions σ_I and σ_B calculated from internal and barrier amplitudes, respectively.

meters, as the scattering amplitude is built up from two components which are sensitive to the values of the potential in different parts of space, and which vary differently with energy. The squared Woods-Saxon form factor used in the present study appears to be suitable for this purpose, although a more flexible form could probably bring further improvement into the quality of the fits. In contrast, when an unappropriate form factor is used (as the usual Woods-Saxon shape seems to be in our case), the potential parameters may present discontinuities as a function of energy[11,22,23] when the relative importance of both components varies markedly in the investigated angular range. In all cases a good description is expected to be more difficult to obtain for angles where f_I and f_B interfere destructively.

Figure 6 presents also the results of similar calculations performed for ^{44}Ca at 36.2 MeV with a modified version of the parametrization B. Potential B has a very small diffuseness in the derivative term [$b_3 = 0.378$ fm in Eq. (6)] and as such introduces many additional turning points near the real axis. This complicates very much the semiclassical interpretation.[32,33]

The modified potential uses the same real part as potential B and an imaginary volume part only, adjusted to give a similar quality of fit to the 36.2 MeV data ($W_v = 25$ MeV, $d_2 = 1.64$ fm, $b_2 = 1$ fm). As one can see, due to the larger absorption in ^{44}Ca the contribution of the internal part of the scattering amplitude is much smaller than for ^{40}Ca and now the barrier part dominates even at backward angles.

A related point of interest is to investigate the range of interdistance for which the cross sections are sensitive to the potential. This was done for the potential B and for ^{40,44}Ca at the 36.2 MeV incident α-particle energy, according to the notch-test technique.[34]

Results are presented in Fig. 7. We see that angular distributions for both ^{40}Ca and ^{44}Ca nuclei are influenced not only by the tail region of the potential ($r > R_{\text{strong absorption}}$) but also by the inner part around $r = 2$ fm. The effect is particularly striking for the ^{40}Ca case. At such small distances, exchange effects are expected to be important; however, according to a prescription recently given by Le Mere *et al.*[35] on the basis of resonating group calculations, one can expect that most of these effects can be included in a central l-independent real potential.

V. CONCLUSIONS

It is demonstrated that both anomalous large angle scattering from ^{40}Ca nuclei and "normal" scattering from ^{44}Ca nuclei can be described as potential scattering in the full range of scattering angles and a wide range of incident energies. No additional resonance amplitude is necessary for this purpose.

The potentials used have squared Woods-Saxon form factors for both real and imaginary parts and energy-independent geometric parameters. Strength parameters of these potentials display a regular energy dependence.

In the low incident energy region absorption of α particles in ^{40}Ca is strongly reduced in comparison with ^{44}Ca. This reduction seems to be located mostly in the surface part of the nucleus (see Fig. 5). Due to the reduced absorption the internal contribution f_I of the semiclassical amplitude is enhanced, and is responsible for the ALAS. The energy dependence of the volume integral of the imaginary potential almost completely vanishes at higher scattering energies although there is indication of some decrease of W with en-

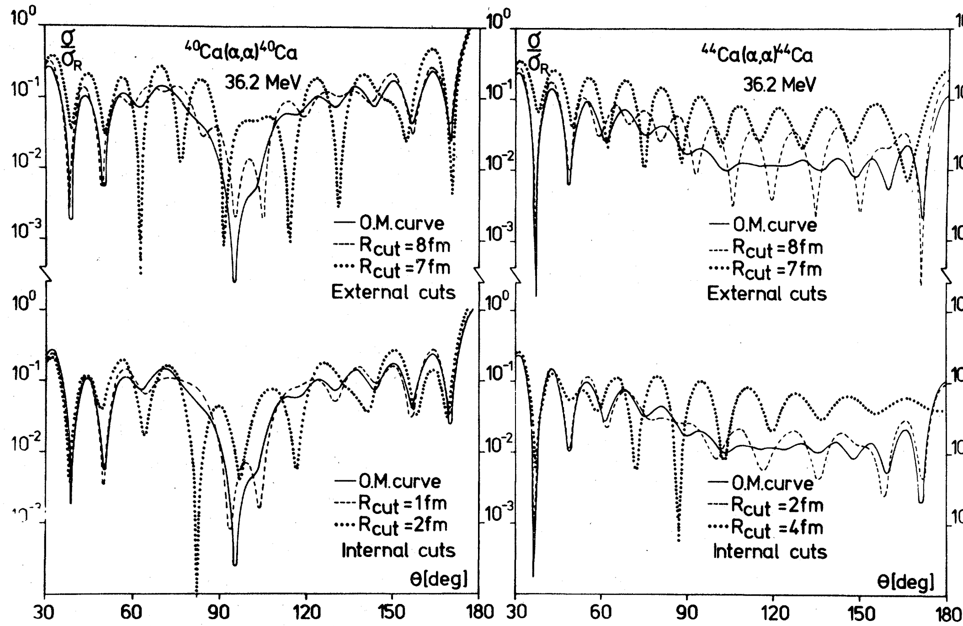

FIG. 7. Results of notch tests performed for ^{40}Ca(α,α)^{40}Ca and ^{44}Ca(α, α)^{44}Ca, respectively. Broken and dotted lines represent modifications of the optical model (O. M.) curve for different values of the internal and external cutoff radius R_{cut}, respectively. The potential B was used for the optical model calculations.

ergy above 100 MeV. A similar tendency was observed in optical model calculations performed by van Oers[36] for the ^{40}Ca + p scattering, where W decreased with energy of protons above about 25 MeV.

The quality of the optical model fits is not as good for ^{40,44}Ca nuclei as for Ni and Zr targets, particularly in the low incident energy region.[21,25,26]

It is likely that further refinements of the potential form factor can still improve the description of scattering from light target nuclei.[23,37]

ACKNOWLEDGMENTS

The authors are indebted to D. M. Brink, D. A. Goldberg, S. Y. Lee, C. Marty, N. Takigawa, and N. S. Wall for many fruitful discussions. Special thanks are due Norman Davison for the critical reading of the manuscript and to the cyclotron staff for the excellent running of the machine. The collaboration of J. Lega, C. Pirart, and P. Wastyn in taking the data is gratefully acknowledged.

---

*Supported in part by the National Science Foundation through the Maria Sklodowska-Curie Fund, Contract No. 01316.

†Chercheur de l'Institut Interuniversitaire des Sciences Nucléaires.

[1]N. S. Wall, A. Budzanowski, G. Heymann, J. W. McVoy, and A. S. Rinat, in Proceedings of the Symposium on Four Nucleon Correlations and Alpha Rotator Structure, Marburg, Germany, edited by R. Stock, 1972 (unpublished).

[2]R. Ceuleneer, H. Oeschler, H. Fuchs, K. A. Eberhard, and K. Grotowski, in Proceedings of the First Louvain-Cracow Seminar on the Alpha-Nucleus Interaction, edited by A. Budzanowski, Cracow, 1973 [INP Report No. 870/PL (unpublished)].

[3]K. Grotowski, in Proceedings of the Fourth EPS Nuclear Physics Divisional Conference-Physics of Medium-Light Nuclei, edited by P. Blasi, Florence, 1977 (unpublished).

[4]F. Michel, Phys. Lett. 60B, 229 (1976).

[5]L. McFadden and G. R. Satchler, Nucl. Phys. 84, 177 (1966).

[6]A. Budzanowski, A. Dudek, R. Dymarz, K. Grotowski, L. Jarczyk, H. Niewodniczanski, and A. Strzalkowski, Nucl. Phys. A126, 369 (1969).

[7]F. Michel and R. Vanderpoorten, Phys. Rev. C 16, 142 (1977).

[8]R. Stock, G. Gaul, R. Santo, M. Bernas, B. Harvey, D. Hendrie, J. Mahoney, J. Sherman, J. Steyaert, and M. Zisman, Phys. Rev. C 6, 1226 (1972).

[9]A. S. Rinat, Phys. Lett. 38B, 281 (1972).

[10]H. Friedrich and K. Langanke, Nucl. Phys. A252, 47

(1975).
[11]H. Löner, H. Eickhoff, D. Frekers, G. Gaul, K. Poppensieker, R. Santo, A. G. Drentje, and L. W. Put, Münster Report No. IKP-9-77 (unpublished).
[12]G. Gaul, H. Lüdecke, R. Santo, H. Schmeing, and R. Stock, Nucl. Phys. A137, 177 (1969).
[13]H. Eickhoff, D. Frekers, H. Löhner, K. Poppensieker, R. Santo, G. Gaul, C. Mayer-Böricke, and P. Turek, Nucl. Phys. A252, 333 (1975).
[14]D. A. Goldberg, Phys. Lett. 55B, 59 (1975).
[15]I. Brissaud and M. K. Brussel, J. Phys. C 3, 481 (1977).
[16]W. T. H. Van Oers, G. J. C. van Niftrik, H. L. Jonkers, and K. W. Brockman, Jr., Nucl. Phys. 74, 469 (1965).
[17]N. Baron, R. F. Leonard, and W. M. Stewart, Phys. Rev. C 4, 1159 (1971).
[18]See AIP document No. PAPS 18-1237-50 for 50 pages of angular distributions of alpha particles. Order by PAPS number and journal reference from American Institute of Physics, Physics Auxiliary Publication Service, 335 East 45th Street, New York, N.Y. 10017. The price is $1.50 for microfiche or $8 for photocopies. Airmail additional. Make checks payable to the American Institute of Physics. This material also appears in Current Physics Microfilm, the monthly microfilm edition of the complete set of journals published by AIP, on the frames immediately following this journal article.
[19]A. Budzanowski, K. Grotowski, M. Grzywacz, and A. Strzalkowski, Institute of Nuclear Physics, Cracow, Progress Report, 1972 (unpublished), pp. 1, 9.
[20]H. H. Chang, B. W. Ridley, J. H. Braid, T. W. Conlon, E. F. Gibson, and N. S. P. King, Nucl. Phys. A270, 413 (1976).
[21]A. Budzanowski, H. Dabrowski, L. Freindl, K. Grotowski, S. Micek, R. Planeta, A. Strzalkowski, M. Bosman, P. Leleux, P. Macq, J.-P. Meulders, and C. Pirart, IFJ Report No. 962/PL, 1977 (unpublished); Phys. Rev. C 17, 951 (1978).
[22]L. W. Put and A. M. J. Paans, Phys. Lett. 49B, 266 (1974).
[23]L. W. Put and A. M. J. Paans, Nucl. Phys. A291, 93 (1977).
[24]P. P. Singh, P. Schwandt, and G. C. Yang, Phys. Lett. 59B, 113 (1975).
[25]Z. Majka, A. Budzanowski, K. Grotowski, and A. Strzalkowski, IFJ Report No. 940/PL, 1977 (to be published in Phys. Rev. C).
[26]Z. Majka and T. Srokowski, Acta Phys. Polonica B9, 75 (1978).
[27]A. Budzanowski, A. Dudek, K. Grotowski, and A. Strzalkowski, Phys. Lett. 32B, 431 (1970); A. Budzanowski, A. Dudek, K. Grotowski, Z. Majka, and A. Strzalkowski, Particles and Nuclei, 6, 97 (1974).
[28]R. H. Bassel, R. M. Drisko, G. R. Satchler, L. L. Lee, J. P. Schiffer, and B. Zeidman, Phys. Rev. B 136, 960 (1964); A. E. Forest, thesis, Oxford report, 1965 (unpublished); P. E. Hodgson, Advan. Phys. 15, 329 (1966).
[29]G. M. Lerner, J. C. Hiebert, L. L. Rutlege Jr., and A. M. Bernstein, Phys. Rev. C 6, 1254 (1972); P. P. Singh, L. W. Put, G. G. Yang, and A. M. J. Paans, in *Proceedings of the International Conference on Nuclear Physics*, *Munich*, 1973, edited by J. de Boer and H. J. Mang (North-Holland, Amsterdam/American Elsevier, New York, 1973), Vol. 1, p. 337.
[30]J. C. Eck, W. J. Thompson, K. Eberhard, J. Schiele, and W. Trombik, Nucl. Phys. A255, 157 (1975).
[31]W. Bertozzi, J. Triar, J. Heisenberg, and J. W. Negele, Phys. Lett. 41B, 408 (1972).
[32]D. M. Brink and N. Takigawa, Nucl. Phys. A279, 159 (1977).
[33]S. Y. Lee, N. Takigawa and C. Marty, Orsay Report No. IPNO/TH 77-4 (unpublished).
[34]P. J. Moffa, C. B. Dover, and J. P. Vary, Phys. Rev. C 13, 147 (1976).
[35]M. Le Mere, R. E. Brown, Y. C. Tang, and D. R. Thompson, Phys. Rev. C 15, 1191 (1977).
[36]W. T. H. Van Oers, Phys. Rev. C 3, 1550 (1971).
[37]E. Friedman and C. J. Batty, Phys. Rev. C 17, 34 (1978); N. S. Wall, A. A. Cowley, R. C. Johnson, and A.M. Kobos, *ibid.* 17, 1315 (1978).